EURASIAN PHYSICAL TECHNICAL JOURNAL

2024, Volume 21, No. 1 (47)

https://doi.org/10.31489/2024No1/114-123

Received: 22/12/2023 Revised: 31/01/2024 Accepted: 07/03/2024 Published online: 29/03/2024

Original Research Article

UDC 532.522.2

NUMERICAL MODELING OF THE PROCESS OF EXTRUSION OF HIGH-VISCOSITY PASTES

Gadirov R.*, Borisov A., Trufanova N., Ragimov E., Artischev S.

Tomsk State University of Control Systems and Radioelectronics, Tomsk, Russia

*Corresponding author: grm882@yandex.ru

Abstract. *This paper provides a theoretical consideration of the process of paste extrusion using a piston dispenser. The paste is considered as a highly viscous suspension of terpineol and silver particle powder. As a result of numerical modeling, the distribution of silver particles in a steady paste flow was obtained. The excess pressure in the piston depending on its speed and the effective width of the track depending on the piston speed were obtained. Modeling showed that the viscosity of the paste has the greatest influence on the extrusion process. Application of the obtained dependencies will allow you to control the paste extrusion process.*

Keywords: extrusion, piston dispenser, silver paste, viscosity, terpineol.

1. Introduction

The application of additive printing technology allowing manufacturing hybrid integrated circuits and devices is gaining popularity due to the reduction in the time expenditures on prototyping and obtaining finished products [1-3]. Studies are being con-ducted in the field of inkjet printing; however, using this technology allows forming only thin-film elements up to 1 μm thick. The inkjet printing technology demonstrates the examples of studying the production of RFID tags [4-7], antennas [8-12] of different types: meander, dual-band, monopole, dipole, ultra-wideband, etc.

Printers that are based on piston, screw and pneumatic extrusion of pastes are used to obtain thick-film elements [1]. The composition and characteristics of the pastes in-tended for piston and screw extrusion differ significantly from the inks used for inkjet printing, as well as from the pastes used for screen printing. The main difference consists in the concentration of solid particles and the material viscosity [2].

The works [13-15] describe the application of piston extrusion of the material used to print microwave antenna systems. The considered antenna systems operate in the range from 2.5 GHz up to 4.7 GHz. The frequency losses of the printed antennas are 5.3 dB at a frequency of 2.5 GHz. The geometric dimensions of the printed antennas are no more than 20×20 mm. A technique used for extracting the frequency electrical parameters of conductive pastes, on the basis of which microstrip lines were formed by piston extrusion, is de-scribed in [16]. A thickness increases in the microstrip line led to a decrease in the frequency losses from 12 dB to 6 dB at a frequency of 1 GHz. A printed multilayer conformal X-band antenna array is considered in [17]. The antenna represents a 32-element X-band superimposed matrix and is manufactured on a surface having several curvilinear lines. The peak antenna gain exceeds 15 dB at a frequency of 10.4 GHz.

Printing the planar components such as inductor, resistor, capacitor is presented in [18,19]. The printed inductor consists of 25 turns. The geometric dimensions of the printed inductor are 14×14 m while the line width is 100 μm and the distance between the lines is about 75 μm. The measured electrical parameters of the inductor have an inductance of 5.42 μH, a resistance of 12.7 kOhm and a capacitance of 50 pF.

Depending on the number of the printed resistor layers, the resistance of the active region varies from 25 Ohms to 650 Ohms. The printed capacitor has a capacity of 322 pF at 1 kHz and a breakdown voltage of 1000 V.

During piston extrusion [3,20], a piston is used to extrude the material being inside the syringe. The extruded volume and the flowrate of the pastes depend on the piston dis-placement inside the syringe. The volume of the extruded pastes and the extrusion rating are related to the piston movement speed [21]. The application of the pastes having different viscosities depends on the power of the drive motor and the mechanical system.

The formation of the printed films structure requires understanding the process of forming a uniform, continuous flow of the paste, its exit from the nozzle and distribution over the substrate. The pressure created in the syringe, the dispenser movement speed and the distance between the nozzle and the substrate influence the printed films quality. The paste extrusion rating depends on such rheological characteristics as viscosity, density, wetting, etc. [22]. Ambient temperature or high pulses of pressure, which can change the outflow rate during the extrusion process, can influence the paste viscosity change.

The dispenser movement rate must be consistent with the linear velocity of the out-flow of the pastes from the nozzle [23]. An extremely high flow rate, as compared to the movement rate of the dispenser, will lead to excessive deformations of the formed films and even to film disruptions [21]. Therefore, the relationship between the movement rate of the dispenser and the linear velocity of the extruded flow, which is a function of a com-plex extrusion process, is crucial for successful deposition and creation of the desired films.

Obtaining high-quality prototypes of printed circuit boards by means of the paste extrusion requires investigating different modes of the printing system operation. This work is devoted to the theoretical study of the capabilities of the dispenser operation during piston extrusion of the paste, consisting of an organic binder (terpineol) and a powder (silver particles).

2. Materials and methods

Let us consider the problem of numerical simulation of squeezing a paste consisting of silver and terpineol particles through a nozzle into the air. Extrusion is carried out in a gravity field using a piston dispenser. (Fig. 1a). This dispenser has axial symmetry, so numerical modeling was carried out in a cylindrical coordinate system. Figure 1b shows the calculated area of the inner part of the dispenser and the air (z_s area).

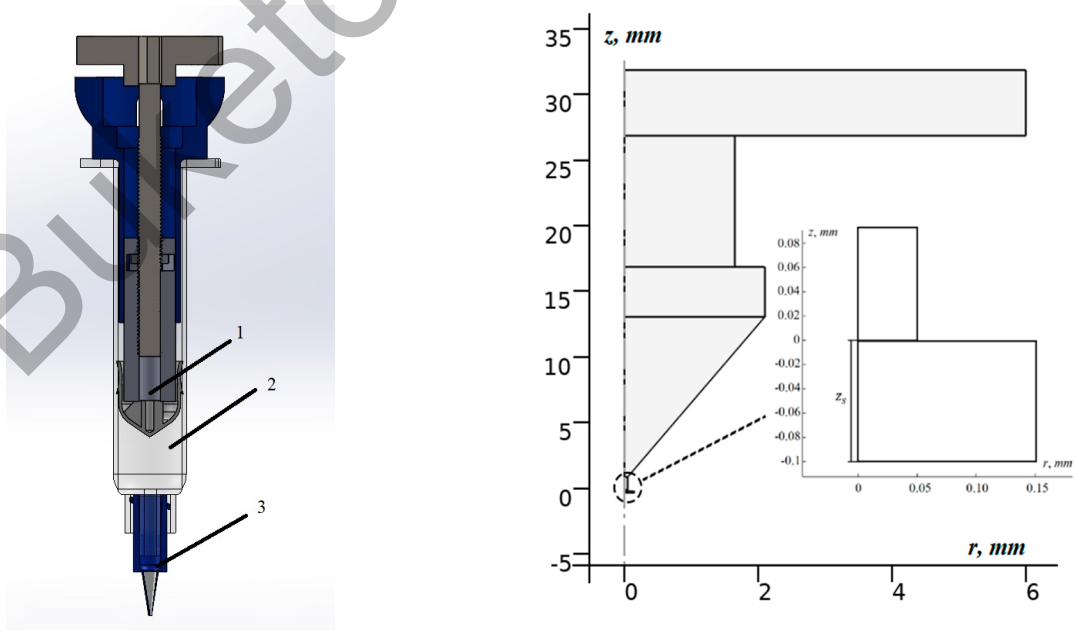

a b

Fig 1. The computational region corresponding to this dispenser (a) 1 is piston, 2 is syringe, 3 is nozzle. Computational region of the model corresponding to the area filled with the paste and air (b).

The left boundary of the calculation area is the axis of symmetry. All other boundaries, with the exception of the top and bottom ones, are considered as impenetrable walls. At the initial moment of time, the dispenser is filled with paste, which is squeezed out under the action of a piston moving at a constant speed along the *z* axis, i.e. a constant paste speed is set perpendicular to the upper boundary. The lower part of the z_s area is an open boundary that air and paste can leave. The pressure at the lower boundary is equal to atmospheric pressure. In this case, for a correct description of the extrusion of paste with silver particles, three-phase medium air/terpineol/silver particles can be considered. Obviously, the case of contact of silver particles with air is not relevant for our task, therefore we will limit ourselves to a description in which only contacts between silver particles with terpineol and terpineol with air are assumed. There are also impermeable walls (syringe surface) where the air/paste/syringe surface area is present.

Let's consider a standard approach to describe our problem based on solving a system of the following equations:

$$\rho\frac{\partial\vec{v}}{\partial t}+\rho(\vec{v}\cdot\nabla)\vec{v}=\nabla\cdot(-p\mathbf{I}+\mathbf{K})+\rho\vec{g}+\vec{F}_\sigma+\vec{F}_\theta \quad (1)$$

$$\frac{\partial\rho}{\partial t}+\nabla\rho\vec{v}=0 \quad (2)$$

$$\frac{\partial\varphi}{\partial t}+\vec{v}\nabla\varphi=\zeta\nabla\cdot\left(\varepsilon\nabla\varphi-\varphi(1-\varphi)\frac{\nabla\varphi}{|\nabla\varphi|}\right)=0 \quad (3)$$

$$\frac{3}{4}\frac{C_d}{d_d}\rho_c|\vec{v}_{slip}|\vec{v}_{slip}=\frac{\rho_2-\rho_d}{\rho_2}\left(\rho_2\frac{\partial\vec{v}}{\partial t}+\rho_2(\vec{v}\cdot\nabla)\vec{v}-\rho_2\vec{g}\right) \quad (4)$$

where Eq. (1) is the Navier-Stokes equation, where Δ is the Laplace operator, ρ is the density, p is the pressure, $\vec{v}=(v^1,v^2)$ is the velocity vector field, $\vec{F}_\sigma$ is the volume force corresponding to surface tension, which characterizes the behavior of the paste at the paste-air interface. This force can be represented in the following form:

$$\vec{F}_\sigma=\sigma\delta\kappa\vec{n},$$

where σ is the terpineol-air surface tension coefficient, $\delta=6|\nabla\varphi|\cdot|\varphi(1-\varphi)|$ is a smooth approximation of the Dirac delta function, κ is the curvature, $\vec{n}$ is the unit vector of the normal to the interface of the terpineol-air phases, $\mathbf{I}$ is the identity matrix, $\mathbf{K}$ is the viscous stress tensor, $\vec{g}$ is the acceleration of gravity. A force arises at the air/paste/syringe surface boundary $\vec{F}_\theta$, directed normal to the paste-air surface:

$$\vec{F}_\theta=\sigma\delta(\vec{n}_{wall}\cdot\vec{n}-\cos(\theta))\vec{n},$$

where $\vec{n}_{wall}$ is the unit vector of the normal to the surface of the syringe.

The viscous stress tensor in the case of a compressible fluid has the form:

$$\mathbf{K}=\mu(\nabla\vec{v}+(\nabla\vec{v})^{\mathrm{T}})-\frac{2}{3}\mu(\nabla\cdot\vec{v})\mathbf{I},$$

where $\nabla\vec{v}$ is the velocity gradient (second-order tensor), $(\ )^{\mathrm{T}}$ indicates the transposition, μ is the dynamic viscosity coefficient.

The air from the paste differs significantly in density and viscosity, therefore, in expressions (1) and (5), the viscosity and density are written as:

$$\rho=\rho_1+(\rho_2-\rho_1)\varphi,$$

$$\mu=\mu_1+(\mu_2-\mu_1)\varphi,$$

where ρ_1, μ_1 are the density and viscosity of the air, ρ_2, μ_2 are the density and viscosity of the paste, φ is a level function obeying equation (3), which is zero in the paste area and one in the air [24], where the ζ parameter characterizes the maximum speed and the ε parameter defines the phase boundary thickness.

The paste velocity $\vec{v}$ depends on the organic binder velocity $\vec{v}_c$ and the relative velocity of the dispersed phase particles $\vec{v}_{slip}$ as follows:

$$\vec{v} = \frac{s_c \rho_c \vec{v}_c + s_d \rho_d (\vec{v}_c + \vec{v}_{slip})}{\rho_2} \quad (5)$$

where $\rho_2 = s_c \rho_c + s_d \rho_d$, s_d takes values from 0 to 1 and characterizes the volume fraction of the dispersed phase particles and $s_c = 1 - s_d$.

Note that at the initial moment of time, silver particles are surrounded by terpineol, and contact between silver is undesirable, therefore, numerical modeling considered only those solutions in which there was no contact between silver particles and air. In this case, the velocity $\vec{v}$ is the velocity of the paste where it is present and the velocity of the air where the paste is absent. The velocity field obeys the corresponding continuity equation Eq. (2). The Eq. (4) describes the behavior of solid particles in a liquid, where C_d is the coefficient characterizing the balance between viscous resistance and buoyancy forces influencing the dispersed phase, d_d is the effective diameter of the dispersed phase particles (solid particles), ρ_d is the dispersed phase density, $\vec{v}_{slip}$ is the velocity of the dispersed phase particles relatively the organic binder, ρ_c is the organic binder density.

A number of approximations of the Rayleigh curve are proposed to describe the transition region for the Reynolds numbers $\mathrm{Re} = \frac{d_d \rho_c}{\mu_2} \left| \vec{v}_{slip} \right|$ that are less than 1000 [25]. The smallest relative error of up to 3 % in the transition region is shown by the Schiller-Neumann approximation [26], according to which the coefficient C_d in the Eq. (4) has the following form:

$$C_d = \frac{24}{\mathrm{Re}} (1 + 0.15 \mathrm{Re}^{0.687})$$

Numerical simulation of the system (1)-(4) was carried out under the following initial and boundary conditions:

1. At the initial moment of time (Figure 2a), the dispenser is completely filled with paste ($\varphi = 1$), and the extrusion area is air ($\varphi = 0$), while the velocity field is zero.

2. As noted above, at the lower boundary of the free space corresponding to the air, the pressure is equal to atmospheric, at the upper boundary a constant value of the paste feed rate $v_{in} = const$ (normal) is set, which corresponds to a constant piston speed. All other boundaries (except for the axis of symmetry) the boundary conditions of an impermeable wall correspond, which is written as follows:

$$\vec{v} \cdot \vec{n} = 0,$$

$$\vec{n} \cdot \left(\varepsilon \nabla \varphi - \varphi (1 - \varphi) \frac{\nabla \varphi}{|\nabla \varphi|} \right) = 0.$$

Let us note that the main geometric characteristics of the internal area of the dispenser are a nozzle diameter of 0.1 mm and a piston diameter of 12 mm.

The paste extrusion was modeled using the COMSOL Multiphysics 6.1 package. In this study, the physical modules Laminar Flow, Level Set and Phase Transport, as well as the calculation modules Phase Initialization and Time-Dependent, were used. An approach that is similar to the one applied in the work was used [26]. The problem was solved using the finite element method, while an appropriate partition was selected for each of the regions, and a finite element grid was selected for each region taking into account the proportion of silver particles in the paste s_d (Fig. 2b).

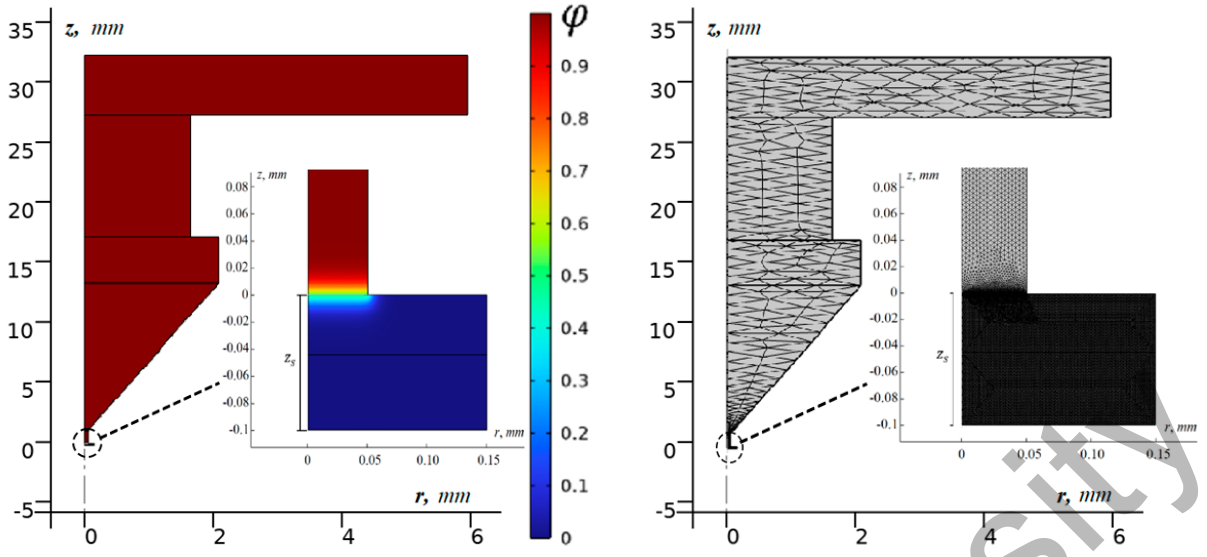

a b

Fig. 2 Initial paste distribution in the calculation area (a) and the grid used for calculation (b)

The (1)-(4) system was numerically modeled using the parameters given in Table 1, considering the influence of surface tension and gravity forces. Table 1 provides the initial physical parameters.

Table 1. Initial parameters for modeling

Parameter	Value	Reference
Terpineol density ρ_c	930 kg/m^3	[27]
Silver density ρ_d	10500 kg/m^3	[28]
Air density ρ_1	1.28 kg/m^3	[29]
Sliver particle size d_d	$2 \cdot 10^{-6}$ m	[30]
Terpineol dynamic viscosity μ_c	0.097 Pa·s	[27]
Air dynamic viscosity μ_1	$1.81 \cdot 10^{-5}$ Pa·s	[29]
Terpineol surface tension	0.033 N/m	[27]
Wetting angle at the interface of terpineol/air/syringe surface	$\pi/2$	[31]

The dynamic viscosity coefficient μ of the paste is of particular interest since it significantly depends on the shear rate $\dot{\gamma}$ in the local region of the space (Fig. 2). This dependence is well described by the Carreau's model [26]:

$$\mu_2 = \mu_{inf} + (\mu_0 - \mu_{inf})(1 + (\lambda\dot{\gamma})^2)^{(n-1)/2} \quad (6)$$

In this case μ_{inf}, μ_0, λ, n are the Carreau's model parameters determined by the experimental data approximation.

A rotary viscometer ViscoQC 300 (Anton Paar, Austria, Graz) in the Heli-Plus configuration was used to determine the dynamic viscosity of the paste; this viscometer allowed obtaining the dependence of the paste dynamic viscosity on the shear rate. The approximation of this dependence in accordance with the Carreau's model Eq. (11) is shown in Fig. 3.

Note that the experimentally obtained dependence (Fig. 3), approximated using the model (6), allows in the process of modeling the extrusion of paste to calculate the viscosity depending on the shear rate $\dot{\gamma}$, which is affected by the redistribution of particles during the movement of the paste.

The following parameters correspond to the dependence presented in Fig. 3: $\mu_{inf} = 0.053$ MPa, $\mu_0 = 0.241$ MPa, $\lambda = 1.151$ s, $n = 0.324$.

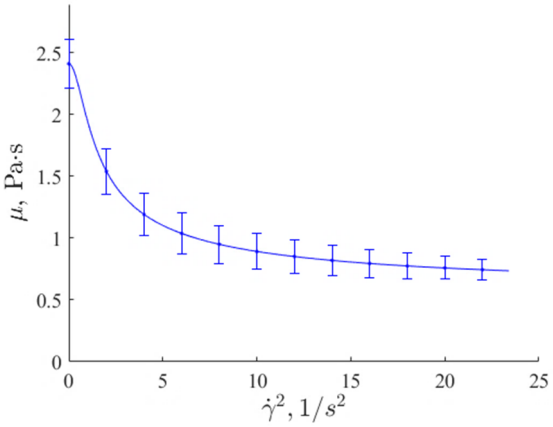

Fig. 3. Approximation of the experimentally obtained dependence of the viscosity on the squared shear velocity with the Carreau's model Eq. (6)

In the Eq. (5), the concept of the volume fraction of the dispersed phase (silver powder) is used, but in experiments, the paste is usually prepared by the mass fraction of the silver powder:

$$\omega = \frac{m_d}{m_d + m_c} \tag{7}$$

where m_d, m_c are the masses of the silver powder and terpineol, respectively.

Knowing the mass fraction of the silver powder allows calculating its volume fraction as follows:

$$s_d = \frac{\rho_c \omega}{\rho_c \omega + \rho_d (1-\omega)} \tag{8}$$

where ρ_d, ρ_c are the density of the silver powder and terpineol, respectively.

3. Results and discussion

The Eq. (1)-(4) system was numerically modeled for different values of the mass fraction of the silver powder Eq. (7) and the piston velocity. Fig. 4a shows the dependences of the volume fraction of the silver powder and the dependence of the function φ on the distance r up to the vertical axis of the dispenser in the steady-state extrusion mode at a distance of $z_s = 0.1$ mm (Fig. 4b) from the outlet section of the nozzle, obtained by means of the numerical modeling. Fig. 4b demonstrates the distribution of the function φ in the computational region of the nozzle and below the nozzle when the mass fraction is ω = 0.7.

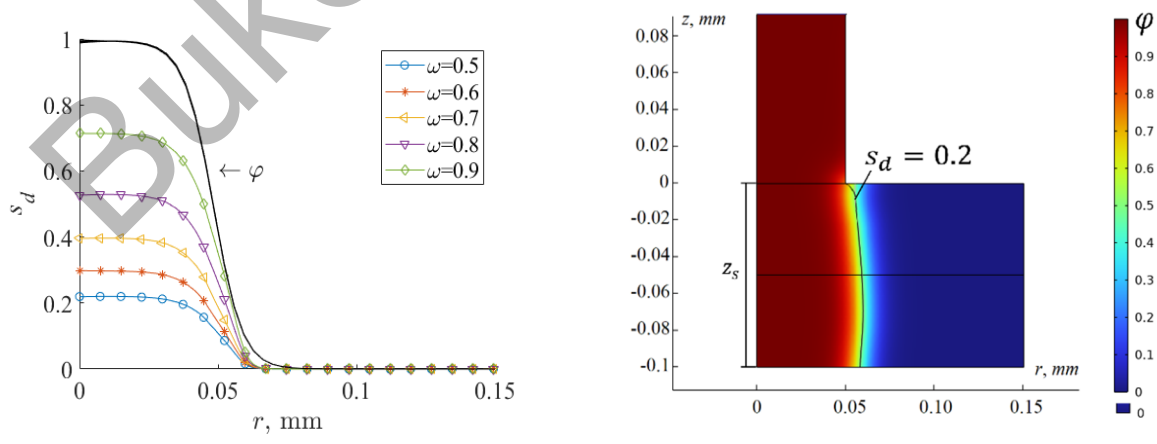

a b

Fig. 4. Dependences of the volume fraction of the silver powder and the dependence of the function φ on the distance r up to the vertical axis of the dispenser in the steady-state extrusion mode at a distance of z_s=0.1 mm from the outlet section of the nozzle (a), distribution of the function φ in the computational region of the nozzle and below the nozzle when the mass fraction is ω=0.7; an additional line of the volume fraction level has been drawn (s_d=0.02) (b).

The function φ type practically does not depend on the mass fraction of the silver powder present in the paste; however, the volume fraction distribution of the silver powder varies significantly. At a sufficiently large interval, when the distance r is increasing, the volume fraction of the dispersed phase remains constant, but it decreases nonlinearly closer to the edge. An increase in the mass fraction of the silver powder obviously leads to a significant increase in the cross-sectional area of the printed tracks, which is proportional to the area under the curves s_d shown in Fig. 3b (the effective width of the track at ω=0.7 is r_e =0.122 mm). The calculations have shown that this dependence is nonlinear, but it is linear in the case of using the volume fraction instead of the mass fraction, which is related to the mass fraction according to the Eq. (8). Let us note that in practice the proposed statements are valid for a stable (debugged) technical process.

Let us consider the dependence of the overpressure (pressure above atmospheric) present on the vertical axis of the dispenser on the distance up to the nozzle section at the outlet as a characteristic of a stable process (Fig. 5a). The maximum pressure inside the dispenser was 0.288 MPa. Changing the piston speed allows obtaining a maximum overpressure that depends on the speed (Fig. 5b).

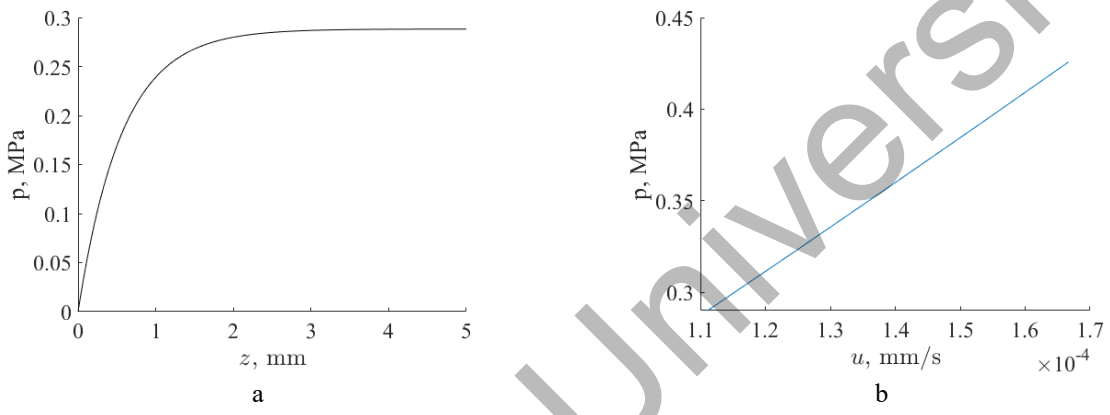

Fig. 5. Dependence of the overpressure present on the vertical axis of the dispenser (the mass fraction is ω=0.7) on the distance to the nozzle section at the outlet (a) and the dependence of the maximum overpressure present in the piston on its velocity (b).

A linear increase in the overpressure accompanied by a piston speed increase leads to a critical value at which the piston will not start to deform; but before reaching this value, the stable operation of the technological process is disrupted because the piston speed increase entails a non-linear increase in the effective width of the track r_e (Fig. 6).

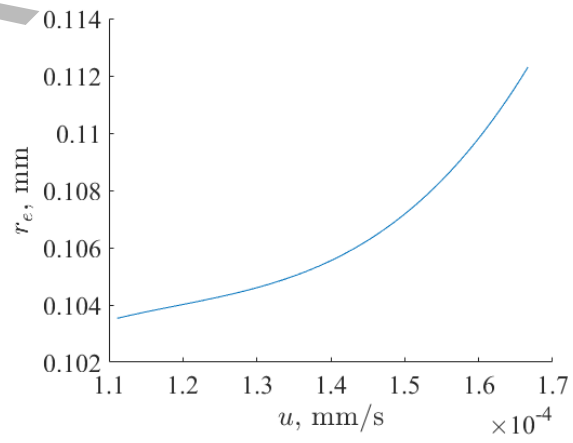

Fig. 6. Dependence of the effective width of the track r_e on the piston speed when ω=0.7.

Fig. 6 shows that the nonlinear growth of the effective width of the track begins at a speed exceeding the value of $1.3 \cdot 10^{-4}$ mm/s. The calculations were additionally carried out in the case of different surface tensions and wetting angles, which proved that the wetting angle did not influence significantly the extrusion process, and the surface tension increase, when other parameters were fixed, led to a strong nonlinearity depending on $r_e(u)$. That is, it is necessary to monitor the terpineol quality when preparing the paste.

According to the numerical modeling results, the effective parameters of the printing system operation are the following. The distance of the dispenser from the substrate is z_s =0.1 mm, the mass fraction of the silver powder in the paste is ω=0.7, the piston speed is $1.1 \cdot 10^{-4}$ mm/s, the maximum pressure in the dispenser is 0.288 MPa, the effective width of the track is r_e =0.122 mm.

4. Conclusions

In this work, a numerical simulation of the piston extrusion process was carried out using the example of terpineol paste and silver particle powder. The main emphasis is placed on obtaining the dependencies for the basic physical quantities on the control parameters and properties of the paste that characterize the dispenser operation in the track printing system.

A mathematical model that allows describing the pastes extrusion has been selected. The numerical modeling has allowed obtaining a set of the parameters of the printing system making the system operation stable. The dependences of the volume fraction of the silver powder on the distance up to the dispenser vertical axis in the steady-state extrusion mode have been obtained. The dependence of the overpressure present on the vertical dispenser axis on the nozzle section distance at the outlet has been studied. The dependences of the maximum over-pressure present in the piston on its speed and the effective width of the track on the piston speed have been determined. The numerical modeling has shown that the paste viscosity influences significantly the extrusion process. An increase in the extrusion speed is shown to increase non-linearly the printed track width. Based on the mathematical model used in the work, a process for manufacturing prototypes of printed circuit boards with subsequent sintering will be developed.

Conflict of interest statement

The authors declare that they have no conflict of interest in relation to this research, whether financial, personal, authorship or otherwise, that could affect the research and its results presented in this paper.

CRediT author statement

Gadirov R.: Writing - Review & Editing, Conceptualization; Borisov A.: Methodology, Formal analysis; Trufanova N.: Writing - Original Draft; Ragimov E.: Visualization; Artischev S: Supervision, Funding acquisition

The final manuscript was read and approved by all authors.

Funding

This research was funded by Ministry of Science and Higher Education of the Russian Federation. State assignment (Goszadanie) – FEWM-2022-0005.

References

1 Divakaran N., Das J.P., PV A.K., Mohanty S., Ramadoss A., Nayak S.K. Comprehensive review on various additive manufacturing techniques and its implementation in electronic devices. *Journal of Manufacturing Systems*, 2022, Vol. 62, pp. 477 – 502. https://doi.org/10.1016/j.jmsy.2022.01.002

2 Hassan K., Nine M.J., Tung T.T., Stanley N., Yap P.L., Rastin H., et al. Functional inks and extrusion-based 3D printing of 2D materials: a review of current research and applications. *Nanoscale*, 2020, Vol. 12, No. 37, pp.19007 – 19042. https://doi.org/10.1039/D0NR04933F

3 Tan H.W., Choong Y.Y.C., Kuo C.N., Low H.Y., Chua C.K. 3D printed electronics: Processes, materials and future trends. *Progress in Materials Science*, 2022, Vol. 127, p. 100945. https://doi.org/10.1016/j.pmatsci.2022.100945

4 Rida A., Yang L., Tentzeris M.M. Design and characterization of novel paper-based inkjet-printed UHF antennas for RFID and sensing applications. *In IEEE Antennas and Propagation Society International Symposium.* HI, USA, 2007, pp. 2749 – 2752. https://doi.org/10.1109/APS.2007.4396104

5 Cook B.S., Mariotti C., Cooper J.R., Revier D., Tehrani B.K., Aluigi L., Roselli L., Tentzeris, M.M. Inkjet-printed, vertically-integrated, high-performance inductors and transformers on flexible LCP substrate. *In 2014 IEEE*

MTT-S International Microwave Symposium (IMS2014), 2014, pp. 1 – 4. https://doi.org/10.1109/MWSYM.2014.6848575

6 Kim S. Inkjet-Printed Electronics on Paper for RF Identification (RFID) and Sensing. *Electronics*, 2020, Vol. 9, No. 10, pp. 1636. https://doi.org/10.3390/electronics9101636

7 Tentzeris M.M., Rida A., Traille A., Lee H., Lakafosis V., Vyas R. Inkjet-printed paper/polymer-based RFID and Wireless Sensor Nodes: The final step to bridge cognitive intelligence, nanotechnology and RF? *XXXth URSI General Assembly and Scientific Symposium.* Istanbul, Turkey, 2011, pp. 1 – 4. https://doi.org/10.1109/URSIGASS.2011.6050690

8 Cook B.S., Fang Y., Kim S., Le T., Goodwin W.B., Sandhage K.H. Inkjet catalyst printing and electroless copper deposition for low-cost patterned microwave passive devices on paper. *Electronic Materials Letters*, 2013, Vol. 9, pp. 669 – 676. https://doi.org/10.1007/s13391-013-3027-0

9 Abutarboush H.F., Shamim A. Wide frequency independently controlled dual-band inkjet-printed antenna. *IET Microwaves, Antennas & Propagation*, 2014, Vol. 8, No. 1, pp. 52 – 56. https://doi.org/10.1049/iet-map.2013.0229

10 Kim S., Cook B.S., Le T., Cooper J., Lee H., Lakafosis V. Inkjet-printed antennas, sensors and circuits on paper substrate. *IET Microwaves, Antennas and Propagation*, 2013, Vol. 7 No. 10, pp. 858 – 668. https://doi.org/10.1049/iet-map.2012.0685

11 Pongpaibool P., Wallada W., Siwamogsatham S. A Thickened-and-Widened Feed Dipole Antenna with an Inductive Matching Loop for a Printed UHF RFID Tag. *In National Electronics and Computer Technology Center*. Sapporo, Japan, 2014, pp. 2092 – 2096. https://doi.org/10.1109/InfoSEEE.2014.6946293

12 Shaker G., Safavi-Naeini S., Sangary N., Tentzeris M.M. Inkjet Printing of Ultrawideband (UWB) Antennas on Paper-Based Substrates. *IEEE Antennas and wireless propagation letters,* 2011, Vol. 10, pp. 111 –114. https://doi.org/10.1109/LAWP.2011.2106754

13 Haerinia M., Noghanian S. Design of Hybrid Wireless Power Transfer and Dual Ultrahigh-Frequency Antenna System. *Proceeding of the URSI International Symposium on Electromagnetic Theory (EMTS)*. California, USA, 2019, 4 p. https://doi.org/10.23919/URSI-EMTS.2019.8931514

14 Haerinia M., Noghanian S. A Printed Wearable Dual-Band Antenna for Wireless Power Transfer. *Sensors*, 2019, Vol. 19, No. 7, p. 1732. https://doi.org/10.3390/s19071732

15 Shadid R., Haerinia M., Noghanian S. Study of Rotation and Bending Effects on a Flexible Hybrid Implanted Power Transfer and Wire-less Antenna System. *Sensors*, 2020, Vol. 20, No. 5, p. 1368. https://doi.org/10.3390/s20051368

16 Trufanova, N.S., Artishchev S.A., Ragimov E.R., Loschilov A.G., Malyshenko A.M.. Technique for extraction of electric frequency parameters of conductive ink. *Journal of Physics: Conference Series*, 2022, Vol. 2291, No. 1, p. 012015. https://doi.org/10.1088/1742-6596/2291/1/012015

17 Kreit E., Steffen T., Aga R., Bartsch C., Wu B.I., Heckman E. Printed multilayer conformal x-band antenna array. *Flexible and Printed Electronics*, 2017, Vol. 2, No. 4, p. 045009. https://doi.org/10.1088/2058-8585/aa940b

18 Correia V., Mitra K.Y., Castro H., Rocha J.G., Sowade E., Baumann R.R., Lanceros-Mendez S. Design and fabrication of multilayer inkjet-printed passive components for printed electronics circuit development. *Journal of Manufacturing Processes*, 2018, Vol. 31, pp. 364 – 371. https://doi.org/10.1016/j.jmapro.2017.11.016

19 Hardin J.O., Grabowski C.A., Lucas M., Durstock M.F., Berrigan J.D. All-printed multilayer high voltage capacitors with integrated processing feedback. *Additive Manufacturing*, 2019, Vol. 27, pp. 327 – 333. https://doi.org/10.1016/j.addma.2019.02.011

20 Kwon K.S., Rahman M.K., Phung T.H., Hoath S.D., Jeong S., Kim J.S. Review of digital printing technologies for electronic materials. *Flexible and Printed Electronics,* 2020, Vol. 5, No. 4, p. 043003. https://doi.org/10.1088/2058-8585/abc8ca

21 Li W., Ghazanfari A., Leu M.C., Landers R.G. Extrusion-on-demand methods for high solids loading ceramic paste in freeform extrusion fabrication. *Virtual and Physical Prototyping*, 2017, Vol. 12, No. 3, pp. 193 – 205. https://doi.org/10.1080/17452759.2017.1312735

22 Chen X.B., Kai J. Modeling of positive-displacement fluid dispensing processes. *IEEE Transactions on Electronics Packaging Manufacturing*, 2004, Vol. 27, No. 3, pp. 157 – 163. https://doi.org/10.1109/TEPM.2004.843083

23 Bruneaux J., Therriault D., Heuzey M.C. Micro-extrusion of organic inks for direct-write assembly. *Journal of Micromechanics and Microengineering*, 2008, Vol. 18, No. 11, p. 115020. https://doi.org/10.1088/0960-1317/18/11/115020

24 COMSOL. The Level Set Method. https://www.comsol.com/forum/thread/attachment/37361/The-level-set-methodfrom-MEMS-Module-5198.pdf.

25 Besagni G., Varallo N., Mereu R. Computational Fluid Dynamics Modelling of Two-Phase Bubble Columns: A Comprehensive Review. *Fluids*, 2023, Vol. 8, No. 3, p. 91. https://doi.org/10.3390/fluids8030091

26 Schmidt G.A., Lin Y.J., Xu Y., Wang D., Yilmaz G., Turng L.S. Viscosity characterization and flow simulation and visualization of polytetrafluoroethylene paste extrusion using a green and biofriendly lubricant. *Polymer Engineering & Science*, 2021, Vol. 61, No. 4, pp. 1050 – 1065. https://doi.org/10.1002/pen.25632

27 Shen F., Dixit M.B., Zaman W., Hortance N., Rogers B., Hatzell, K.B. Composite electrode ink formulation for all solid-state batteries. *Journal of The Electrochemical Society*, 2019, Vol. 166, No. 14, p. A3182. https://doi.org/10.1149/2.0141914jes

28 Slistan-Grijalva A., Herrera-Urbina R., Rivas-Silva J.F., Ávalos-Borja M., Castillón-Barraza F.F., Posada-Amarillas A. Classical theoretical characterization of the surface plasmon absorption band for silver spherical nanoparticles suspended in water and ethylene glycol. *Physica E: Low-dimensional Systems and Nanostructures*, 2005 Vol. 27, No. 1 – 2, pp. 104 – 112. https://doi.org/10.1016/j.physe.2004.10.014

29 El-Said M., Bhuse V., Arendsen A. An empirical study to investigate the effect of air density changes on the DSRC performance. *Procedia computer science*, 2017, Vol. 114, pp. 523 – 530. https://doi.org/10.1016/j.procs.2017.09.025

30 Won H.I., Nersisyan H., Won C.W., Lee J.M., Hwang J.S. Preparation of porous silver particles using ammonium formate and its formation mechanism. *Chemical Engineering Journal*, 2010, Vol. 156, No. 2, pp. 459 – 464. https://doi.org/10.1016/j.cej.2009.10.053

31 Fujasova-Zednikova M., Vobecka L., Vejrazka J. Effect of solid material and surfactant presence on interactions of bubbles with horizontal solid surface. *The Canadian Journal of Chemical Engineering*, 2010, Vol. 88, No. 4, pp. 473 – 481. https://doi.org/10.1002/cjce.20326

AUTHORS' INFORMATION

Gadirov, R. – PhD, Head of laboratory, Tomsk State University of Control Systems and Radioelectronics, Tomsk, Russia; ORCID iD: 0000-0003-3953-3384; grm882@yandex.ru

Borisov, A. – PhD, Senior Researcher, Tomsk State University of Control Systems and Radioelectronics, Tomsk, Russia; ORCID iD: 0000-0003-1752-1649; borisov@phys.tsu.ru

Trufanova, N. – Graduate student, Junior researcher, Tomsk State University of Control Systems and Radioelectronics, Tomsk, Russia; ORCID iD: 0000-0002-2055-5316; natalia.s.trufanova@tusur.ru

Ragimov, E. – Master student, Engineer, Tomsk State University of Control Systems and Radioelectronics, Tomsk, Russia; ORCID iD: 0009-0007-9946-2377; ragimov_30@mail.ru

Artischev, S. – PhD, head of laboratory, Tomsk State University of Control Systems and Radioelectronics, Tomsk, Russia; ORCID iD: 0000-0002-9905-621X; sergei.a.artishchev@tusur.ru